Supplementary material

Facile Fabrication of Pyrazine-linked Metallophthalocyanine-based Porous Organic Polymers (PyMPc-POPs) and their Reduced Graphene Oxide (rGO) Hybrids for Light-Driven CO_2 Cycloaddition

Boxin Zhang[a], Tao Wei[a], Minghui Chen[a], Yunhao Xu[a], Zhaoxue Sun[a], Minghao Duo[a], Bao Zhang[*a,b]

a School of Chemical Engineering and Technology, Tianjin University, Tianjin 300350, PR China.

b Tianjin Collaborative Innovation Center of Chemical Science and Engineering, Tianjin 300072, PR China.

* E-mail: baozhang@tju.edu.cn

Materials and Measurements

Materials. Unless otherwise stated, all the chemicals and solvents are commercially available from local chemical distributors, and used without further purification.

Measurements. Liquid 1D ^{1}H NMR spectra of all monomers were recorded on a Bruker AVANCE IIITM HD 400 MHz NanoBAY. 600 M solid ^{13}C NMR spectra were measured on the JEOL JNM ECZ600R. Powder X ray diffraction (PXRD) data were collected on Rigaku Smartlab 8KW using Cu Kα radiation at 40 kV, 40 mA power. Fourier-transform infrared (FT-IR) spectra was recorded on Nicolet 6700 instrument (600-3500 cm^{-1} region). Thermogravimetric analysis (TGA) was carried out on a Netzsch TG 209F3 analyzer with a heat rate of 10 °C in nitrogen atmosphere. A Field Emission Scanning Electron Microscope (FE-SEM) images and energy dispersive spectroscopy (EDS) were obtained with a Regulus 4800 electron microscope (Japan, Hitachi Limited). Transmission electron microscopies (TEM), was performed using JEOL model JEM-F200. The X-ray photoelectron spectroscopy (XPS) analysis was obtained by ESCALAB 250xi, Thermo Scientific. UV-Visible diffuse reflectance spectra (DRS) were obtained by PE lambda 1050 with an integrating sphere mode. The steady photoluminescence data were measured by HORIBA-QM steady state/transient state fluorescence spectrometer in the solid state. Nitrogen adsorption and carbon dioxide adsorption of POPs were measured by Specific Surface Area and Porosity Analyzer. In situ EPR was performed using Bruker EMXplus. Electrochemical properties of the material frameworks were measured through a three-electrode system in an electrochemical workstation with a brand of CHI660d, Chenhua. For these measurements, 2 mg POPs was dispersed into the mixed solvent of 0.75 mL Isopropanol and 0.25 mL 5wt% Nafion aqueous solution via the ultrasonic treatment for 60 min. After that, 20 μL suspension was deposited onto clean Φ3 GCE as the working electrode. And the Ag/AgCl electrode worked as the reference electrode and Pt flake was acted as the counter electrode. Na_2SO_4 aqueous solution (0.1 M) acted as electrolyte during the measurements.

By introducing a vacuum layer along the z-direction, DFT calculations were performed

on the single-layer metal polyphthalocyanine-based porous organic polymer (POP)[1]. The computations were implemented using the CP2K-2024.1 software package, with geometric optimization conducted at the PBE/DZVP-MOLOPT-SR-GTH level to yield the optimized structure. Based on the optimized structure, single-point energy calculations for the ground and excited states were carried out at the HSE06/DZVP-MOLOPT-SR-GTH level[2]. Subsequently, the electron-hole distribution in the first excited singlet state was derived via post-processing with the Multiwfn program[3-5].

The optical band gap was calculated from the UV-vis diffuse reflectance spectra (DRS) using the Tauc plot method after transformation with the Kubelka-Munk function. The optical band gaps were estimated by assuming direct allowed transitions

$$(\alpha h\nu)^n = A(h\nu - Eg)$$

where α is the absorption index, h is the Planck constant, ν is the light frequency, Eg is the band gap of the semiconductor, and A is a constant. The value of n depends on the type of semiconductor, and n is taken as 2 in this work.

.

Synthesis Methods

Pyrazine-2,3,5,6-tetracarbonitrile (TCNP)

Synthesis was carried out using a modified literature procedure[6]. To a solution of diaminomaleonitrile (0.02 mol, 2.16 g) in 30 mL of trifluoroacetic acid, 2,3-dichloro-5,6-dicyano-1,4-benzoquinone (0.01 mol, 2.27 g) was added portion-wise at room temperature and the mixture was stirred at room temperature for 4 h, then warmed to 70 °C and filtered, washed with trifluoroacetic acid and water. The precipitate containing mostly pyrazine-2,3,5,6tetracarbonitrile, 6-aminopyrazine-2,3,5-tricarbonitrile and 2,3-dichloro-5,6-dicyanohydroquinone was purified by boiling in toluene followed by hot filtration. The filtrate was evaporated under reduced pressure to dry, washed with water, chloroform and dried at room temperature under high vacuum.

The procedure for fabrication of hybrid monomer precursors TCNP@rGO-X (where X = 5, 10, 15, and 20, denoting the mass percentage of rGO relative to TCNP).

Firstly, a specified amount of reduced graphene oxide (rGO) with varying mass ratios (X = 5%, 10%, 15%, and 20%) was dispersed in deionized water (100 mL) and subjected to ultrasonication for 10 minutes. The resulting dispersion was then stirred vigorously for 4 hours at room temperature to obtain a homogeneous suspension. Separately, 180 mg (1 mmol) of TCNP was dissolved in 0.5 mL of N,N-dimethylformamide (DMF) with gentle heating at 60 °C to afford a clear solution. The TCNP/DMF solution was added dropwise over a period of 5-10 min to the prepared rGO dispersions under continuous stirring to ensure gradual and uniform contact. The mixture was stirred for 2 hours at room temperature to facilitate the effective deposition of TCNP molecules onto the rGO surface. The solid was then collected by vacuum filtration, thoroughly washed with deionized water, and dried under vacuum at 60 °C for 12 hours. This procedure yielded TCNP@rGO-X composite powders in nearly quantitative amounts for each designated rGO loading[7].

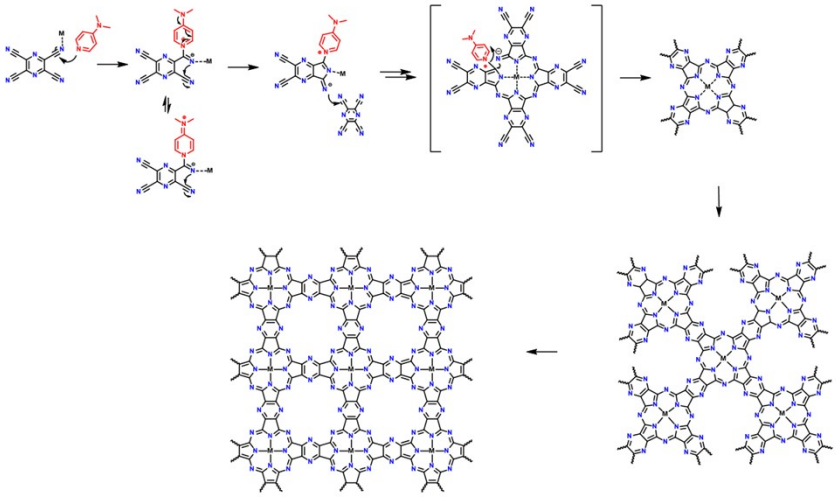

Figure S1. Proposed mechanism for the formation of polyphthalocyanine.

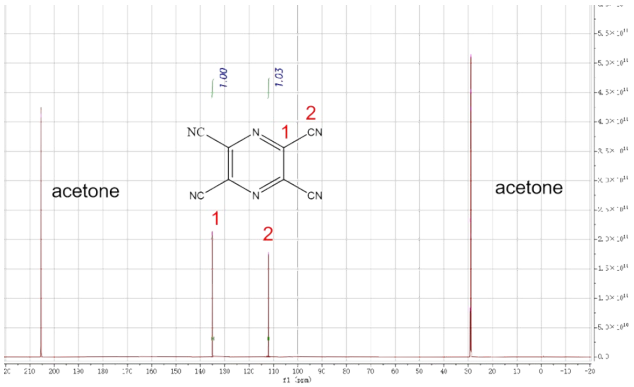

Figure S2. ^{13}C NMR of TCNP molecule.

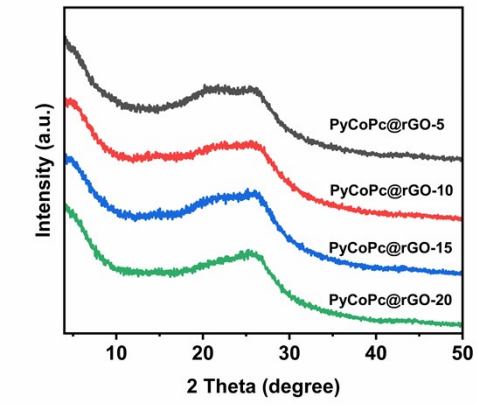

Figure S3. The experimental PXRD patterns of PyCoPc@rGO.

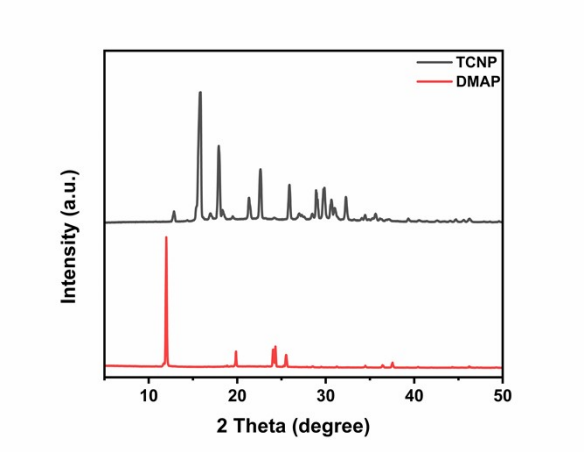

Figure S4. The experimental PXRD patterns of TCNP and DMAP.

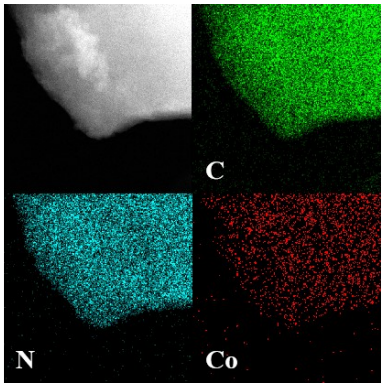

Figure S5. The EDS elemental mapping (C, N and Co) of PyCoPc.

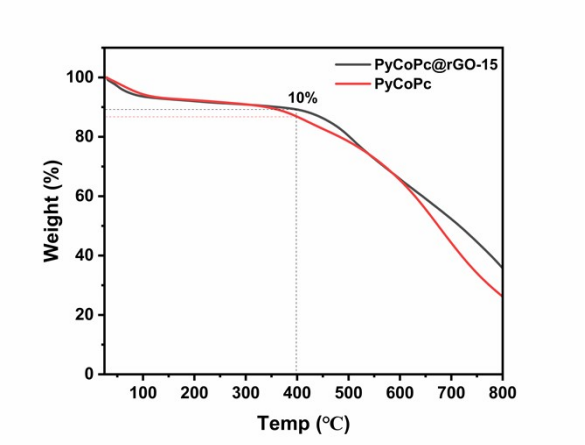

Figure S6. The TGA curves of PyCoPc and PyCoPc@rGO-15.

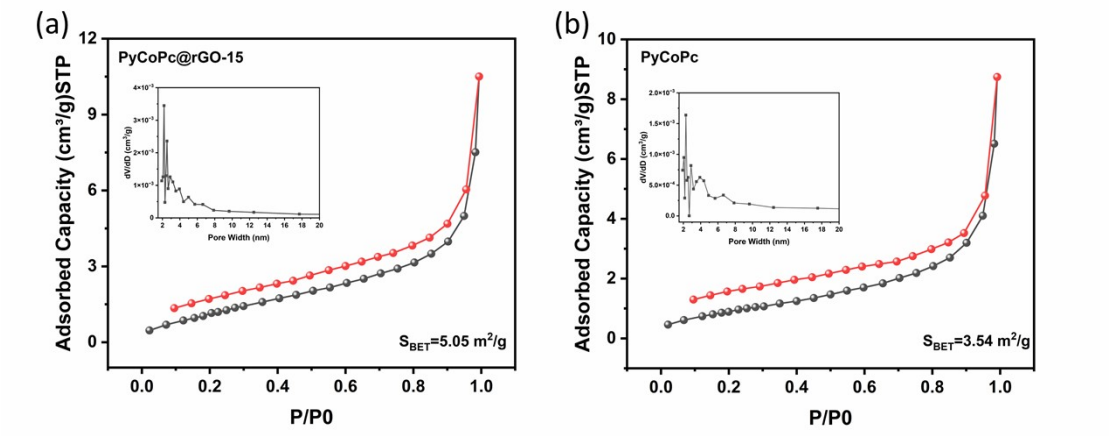

Figure S7. The Nitrogen sorption isotherm curves and the pore size distribution of (a) PyCoPc@rGO-15 and (b) PyCoPc.

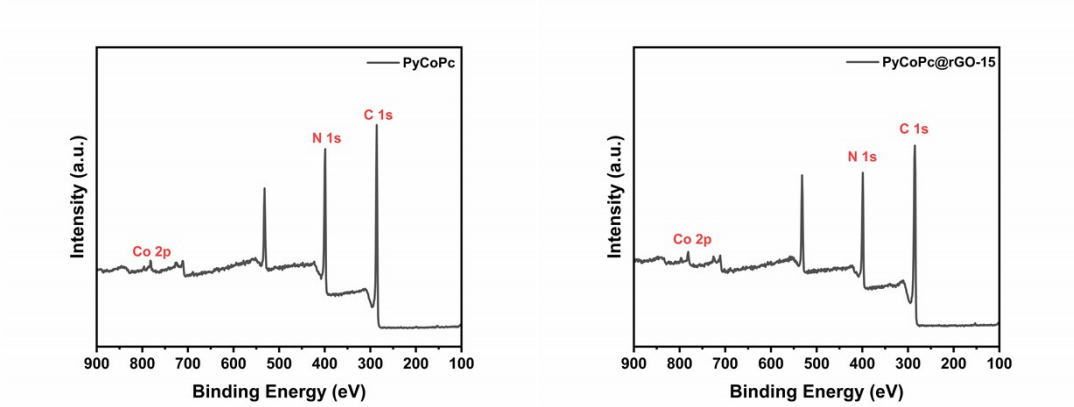

Figure S8. XPS of PyCoPc and PyCoPc@rGO-15.

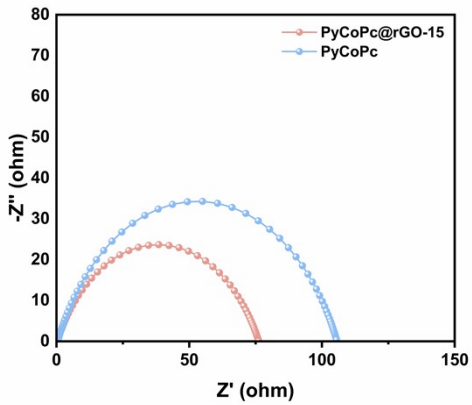

Figure S9. Electrochemical impedance spectroscopy (EIS) Nyquist plots of PyCoPc and PyCoPc@rGO-15.

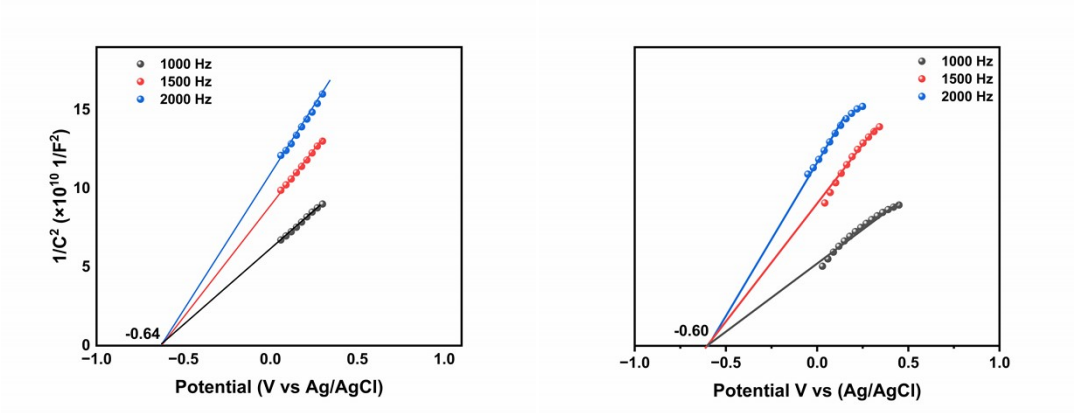

Figure S10. Mott-Schottky curves of PyCoPc and PyCoPc@rGO-15.

Table S1. Chemical shifts (δ , ppm) for the integrated protons in the epoxides and corresponding carbonates (in $CDCl_3$)

Epoxide	δH (epoxide, 1Hc)	δH (carbonate, 1Hc')
	2.62	4.37
	2.61	4.31
	2.41	4.03
	2.72	4.23
	2.72	4.53
	2.53	4.45
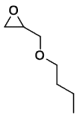	2.54	4.46

Table S2. The conversion rate of ECH after 12 h irradiation with a 30 W LED over a series of POPs-based catalysts

30W-12h	Catalyst	Cocatalyst	Conversion/%
1	PyCoPc	1mmol TBAB	65.8
2	PyCoPc@rGO-5	1mmol TBAB	71.8
3	PyCoPc@rGO-10	1mmol TBAB	74.2
4	PyCoPc@rGO-15	1mmol TBAB	77.8
5	PyCoPc@rGO-20	1mmol TBAB	74.3

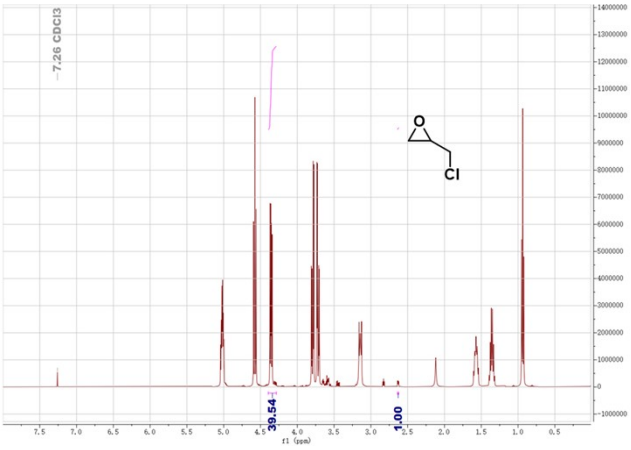

Figure S11. ^{1}H NMR (400 MHz, $CDCl_3$) spectrum of reaction system in Figure 5b entry 1

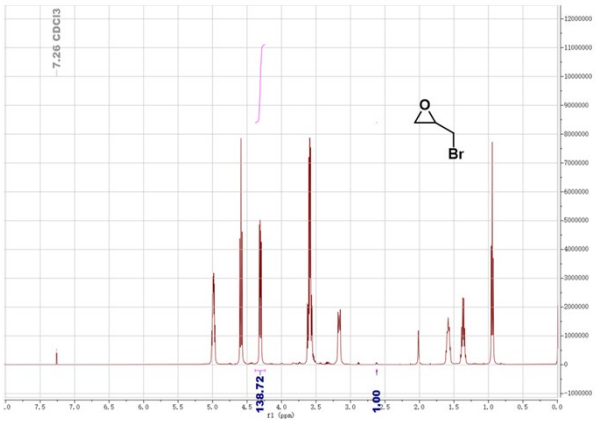

Figure S12. ^{1}H NMR (400 MHz, $CDCl_3$) spectrum of reaction system in Figure 5b entry 2

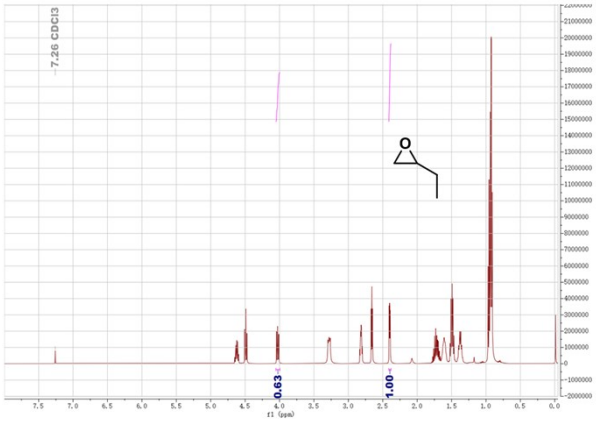

Figure S13. ^{1}H NMR (400 MHz, $CDCl_3$) spectrum of reaction system in Figure 5b entry 3

Figure S14. ^{1}H NMR (400 MHz, $CDCl_3$) spectrum of reaction system in Figure 5b entry 4

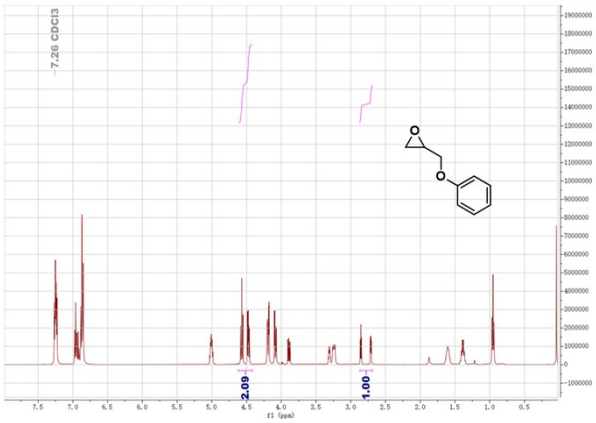

Figure S15. ^{1}H NMR (400 MHz, $CDCl_3$) spectrum of reaction system in Figure 5b entry 5

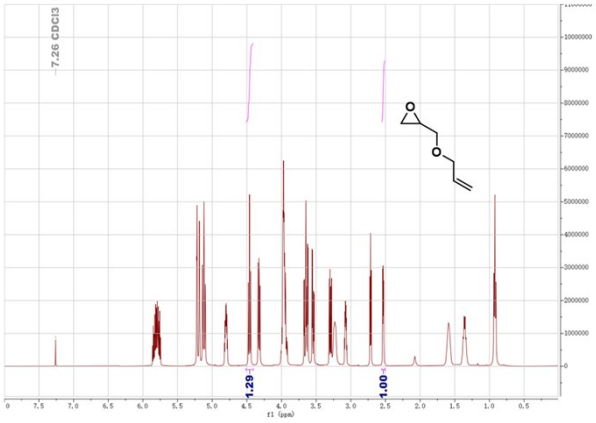

Figure S16. ^{1}H NMR (400 MHz, $CDCl_3$) spectrum of reaction system in Figure 5b entry 6

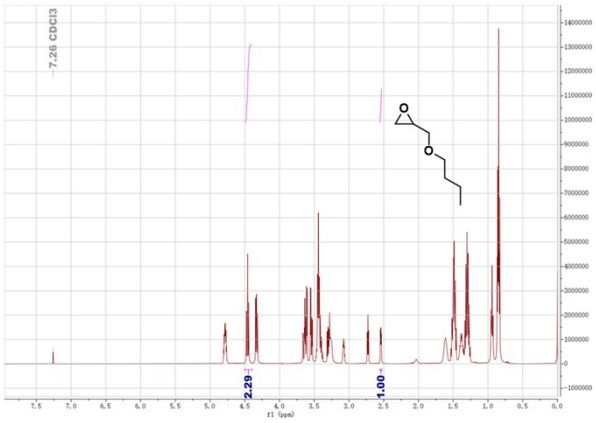

Figure S17. ^{1}H NMR (400 MHz, $CDCl_3$) spectrum of reaction system in Figure 5b entry 7

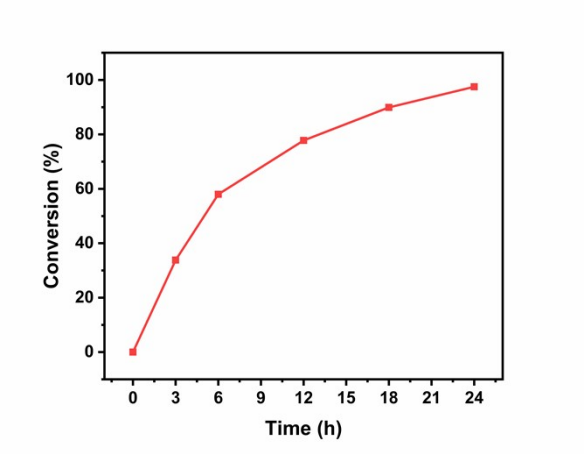

Figure S18. Time course of photocatalytic CO_2 cycloaddition on PyCoPc@rGO-15 photocatalysts.

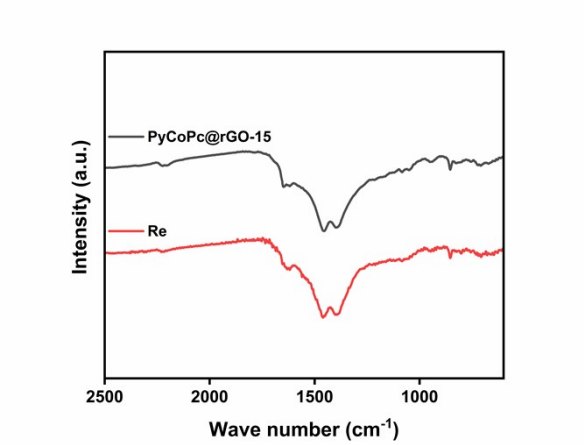

Figure S19. The FT-IR spectra of PyCoPc@rGO-15 after successive catalytic cycles

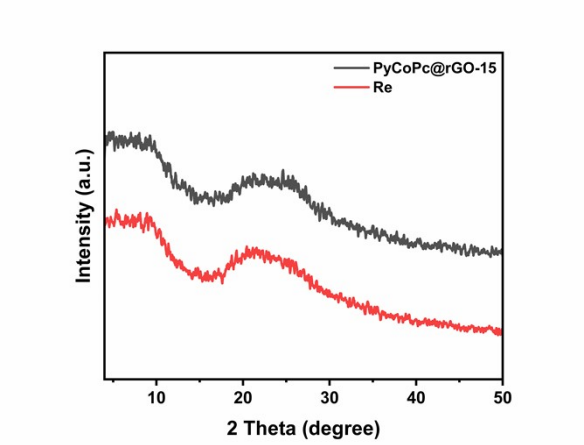

Figure S20. The XRD of PyCoPc@rGO-15 after successive catalytic cycles

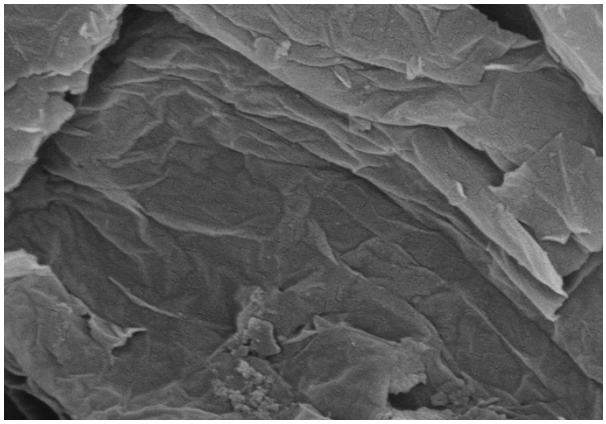

Figure S21. The SEM of PyCoPc@rGO-15 after successive catalytic cycles

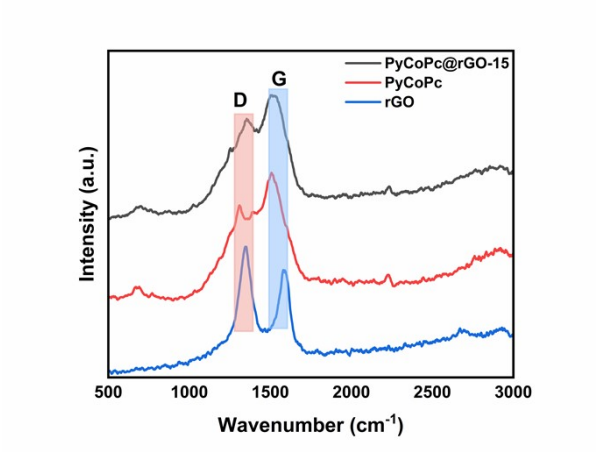

Figure S22 The Raman of PyCoPc@rGO-15, PyCoPc and rGO

Table S3. Atom contribution to hole and electron.

	Hole:	Electron:	Overlap:	Diff.:
1(C)	0.33%	1.27%	0.65%	0.94%
2(N)	0.29%	0.20%	0.24%	-0.09%
3(N)	0.29%	0.20%	0.24%	-0.09%
4(N)	0.28%	1.88%	0.73%	1.60%
5(N)	0.28%	1.88%	0.73%	1.60%
6(C)	1.56%	0.52%	0.90%	-1.03%
7(C)	0.27%	0.07%	0.14%	-0.20%
8(C)	0.33%	1.27%	0.65%	0.94%
9(C)	1.56%	1.20%	1.37%	-0.36%
10(C)	1.56%	0.52%	0.90%	-1.03%
11(N)	0.35%	1.48%	0.72%	1.13%
12(C)	1.56%	0.52%	0.90%	-1.04%
13(C)	1.56%	1.20%	1.37%	-0.37%
14(N)	0.35%	1.48%	0.72%	1.13%
15(C)	1.56%	1.20%	1.37%	-0.37%
16(N)	0.35%	1.48%	0.72%	1.13%
17(C)	0.33%	1.27%	0.65%	0.94%
18(C)	0.27%	0.07%	0.14%	-0.20%
19(C)	0.27%	0.07%	0.14%	-0.20%
20(C)	1.56%	0.52%	0.90%	-1.03%
21(C)	1.56%	1.20%	1.37%	-0.36%
22(N)	0.35%	1.48%	0.72%	1.13%
23(C)	0.33%	1.27%	0.65%	0.94%
24(C)	0.27%	0.07%	0.14%	-0.20%
25(N)	0.85%	0.15%	0.36%	-0.69%
26(N)	0.85%	0.15%	0.36%	-0.70%
27(N)	1.17%	0.25%	0.54%	-0.92%
28(N)	1.17%	0.25%	0.54%	-0.92%
29(C)	0.37%	1.11%	0.64%	0.74%
30(N)	0.39%	0.15%	0.24%	-0.25%
31(N)	0.39%	0.15%	0.24%	-0.25%
32(N)	0.39%	1.38%	0.73%	0.99%
33(N)	0.39%	1.38%	0.73%	0.99%
34(C)	2.15%	0.38%	0.91%	-1.77%
35(C)	0.37%	0.06%	0.15%	-0.32%
36(C)	0.37%	1.12%	0.64%	0.74%
37(C)	2.15%	0.89%	1.38%	-1.25%
38(C)	2.15%	0.38%	0.91%	-1.77%
39(N)	0.48%	1.05%	0.71%	0.57%
40(C)	2.15%	0.38%	0.91%	-1.77%
41(C)	2.15%	0.89%	1.38%	-1.25%
42(N)	0.48%	1.05%	0.71%	0.57%
43(C)	2.15%	0.89%	1.38%	-1.25%
44(N)	0.48%	1.05%	0.71%	0.57%
45(C)	0.37%	1.12%	0.64%	0.74%
46(C)	0.37%	0.06%	0.15%	-0.32%
47(C)	0.37%	0.06%	0.15%	-0.32%
48(C)	2.15%	0.38%	0.91%	-1.77%
49(C)	2.15%	0.89%	1.38%	-1.25%
50(N)	0.48%	1.05%	0.71%	0.57%
51(C)	0.37%	1.12%	0.64%	0.74%

	Hole:	Electron:	Overlap:	Diff.:
52(C)	0.37%	0.06%	0.15%	-0.32%
53(N)	1.17%	0.12%	0.38%	-1.05%
54(N)	1.17%	0.12%	0.38%	-1.05%
55(N)	1.17%	0.25%	0.54%	-0.92%
56(N)	1.17%	0.25%	0.54%	-0.92%
57(C)	0.33%	1.28%	0.65%	0.95%
58(N)	0.29%	0.20%	0.24%	-0.09%
59(N)	0.29%	0.20%	0.24%	-0.09%
60(N)	0.28%	1.90%	0.73%	1.62%
61(N)	0.28%	1.90%	0.73%	1.62%
62(C)	1.56%	0.53%	0.91%	-1.03%
63(C)	0.27%	0.07%	0.14%	-0.20%
64(C)	0.33%	1.28%	0.65%	0.95%
65(C)	1.56%	1.21%	1.38%	-0.35%
66(C)	1.56%	0.53%	0.91%	-1.03%
67(N)	0.35%	1.50%	0.72%	1.15%
68(C)	1.56%	0.53%	0.91%	-1.03%
69(C)	1.56%	1.21%	1.38%	-0.35%
70(N)	0.35%	1.50%	0.72%	1.15%
71(C)	1.56%	1.21%	1.38%	-0.35%
72(N)	0.35%	1.50%	0.72%	1.15%
73(C)	0.33%	1.28%	0.65%	0.95%
74(C)	0.27%	0.07%	0.14%	-0.20%
75(C)	0.27%	0.07%	0.14%	-0.20%
76(C)	1.56%	0.53%	0.91%	-1.03%
77(C)	1.56%	1.21%	1.38%	-0.35%
78(N)	0.35%	1.50%	0.72%	1.15%
79(C)	0.33%	1.28%	0.65%	0.95%
80(C)	0.27%	0.07%	0.14%	-0.20%
81(N)	0.85%	0.15%	0.36%	-0.69%
82(N)	0.85%	0.15%	0.36%	-0.70%
83(N)	1.17%	0.26%	0.55%	-0.91%
84(N)	1.17%	0.26%	0.55%	-0.91%
85(C)	0.37%	1.13%	0.65%	0.76%
86(N)	0.39%	0.15%	0.24%	-0.24%
87(N)	0.39%	0.15%	0.24%	-0.24%
88(N)	0.39%	1.39%	0.74%	1.00%
89(N)	0.39%	1.39%	0.74%	1.00%
90(C)	2.15%	0.39%	0.91%	-1.76%
91(C)	0.37%	0.06%	0.15%	-0.32%
92(C)	0.37%	1.13%	0.65%	0.76%
93(C)	2.14%	0.90%	1.39%	-1.24%
94(C)	2.15%	0.39%	0.91%	-1.76%
95(N)	0.48%	1.06%	0.72%	0.58%
96(C)	2.15%	0.39%	0.91%	-1.77%
97(C)	2.15%	0.90%	1.39%	-1.24%
98(N)	0.48%	1.06%	0.72%	0.58%
99(C)	2.15%	0.90%	1.39%	-1.24%
100(N)	0.48%	1.06%	0.72%	0.58%
101(C)	0.37%	1.13%	0.65%	0.76%
102(C)	0.37%	0.06%	0.15%	-0.32%
103(C)	0.37%	0.06%	0.15%	-0.32%
104(C)	2.15%	0.39%	0.91%	-1.76%
105(C)	2.15%	0.90%	1.39%	-1.24%

	Hole:	Electron:	Overlap:	Diff.:
106(N)	0.48%	1.06%	0.71%	0.58%
107(C)	0.37%	1.13%	0.65%	0.76%
108(C)	0.37%	0.06%	0.15%	-0.32%
109(N)	1.17%	0.12%	0.38%	-1.05%
110(N)	1.17%	0.12%	0.38%	-1.05%
111(N)	1.17%	0.26%	0.55%	-0.91%
112(N)	1.17%	0.26%	0.55%	-0.91%
113(Co)	0.12%	3.80%	0.67%	3.68%
114(Co)	0.09%	5.15%	0.68%	5.06%
115(Co)	0.12%	3.71%	0.66%	3.59%
116(Co)	0.09%	5.02%	0.67%	4.93%

Sum of hole shown above: 100.00%. Sum of electron shown above: 100.00

Table S4 Comparison of photocatalytic CO_2 cycloaddition activities for typical photocatalysts

Entry	Catalyst	Reaction system	Light irridiation	T/°C	P/bar	Time/h	Conversion/%	Ref
1	PyCoPc@rGO-15	TBAB (1.0 mmol), ECH (12.75 mmol)	30W White LED	r.t.	1	24	97.5	This work
2	CoPc/TiO_2	CH3CN+MeOH (15 mL), TBAB (1.0 mmol), ECH (12.75 mmol),	20W White LED	r.t.	1	24	94	8
3	Co-HOF	TBAB (0.028 mmol)	400 W halogen lamp	80	/	24	99.9	9
4	Co-s-ZIS	TBAB (0.1mmol)	Visible light	r.t.	1	24	97.5	10
5	Fe-DBP(Co)	TBAB (1.0mmol)	1000 W xenon lamp	r.t.	1	12	97.1	11
6	Zn@MA-POP	TBAB (0.160 g), ECH (0.5 ml)	250 W xenon lamp	r.t.	1	8	26	12
7	Fe-BTCH2O-130	CH3CN (3 mL) TBAB (0.2 mmol), ECH (0.2 mmol)	30 W blue LED	r.t.	1	8	92	13
8	USTC-253-TFA	TBAB (1.86 mmol), ECH (28.6 mmol)	/	r.t.	1	72	38.2	14
9	UiO-bpydc(Zn)	DMF (3ml) TBAB (0.5 mmol), ECH (0.1 mmol)	300 W xenon lamp	r.t.	1	9	93	15
10	Zn SA-NC	DMF (3ml) TBAB (0.1 mmol), ECH (0.15 mmol)	3000 W/m^2	65	1	16	99	16
11	HPC-800	DMF (3ml) TBAB (0.1 mmol), ECH (0.15 mmol)	3000 W/m^2	60	1	10	96	17

References

1 T. D. Kühne, M. Iannuzzi, M. Del Ben, V. V. Rybkin, P. Seewald, F. Stein, T. Laino, R. Z. Khaliullin, O. Schütt, F. Schiffmann, D. Golze, J. Wilhelm, S. Chulkov, M. H. Bani-Hashemian, V. Weber, U. Borštnik, M. Taillefumier, A. S. Jakobovits, A. Lazzaro, H. Pabst, T. Müller, R. Schade, M. Guidon, S. Andermatt, N. Holmberg, G. K. Schenter, A. Hehn, A. Bussy, F. Belleflamme, G. Tabacchi, A. Glöß, M. Lass, I. Bethune, C. J. Mundy, C. Plessl, M. Watkins, J. VandeVondele, M. Krack and J. Hutter, J. Chem. Phys., 2020, 152, 194103.

2 R. Y. Liu, D. Zhao, S. L. Ji, H. P. Shao, Y. Z. Chen, M. J. Feng, T. Wang, J. Li, M. Lin, T. C. Sum, N. Yan, S. Seki and D. L. Jiang, Nat. Mater., 2025, 1–13.

3 T. Lu, J. Chem. Phys., 2024, 161, 82503.

4 T. Lu and F. W. Chen, J. Comput. Chem., 2012, 33, 580–592.

5 Z. Y. Liu, T. Lu and Q. X. Chen, Carbon, 2020, 165, 461–467.

6 T. G. Witkowski, E. Sebastiao, B. Gabidullin, A. Hu, F. Zhang and M. Murugesu, ACS Appl. Energy Mater., 2018, 1, 589–593.

7 M. H. Chen, Z. X. Sun, T. Wei, B. X. Zhang, K. Guo, Y. Q. Feng and B. Zhang, Chem. Eng. J., 2025, 508, 160982.

8 P. K. Prajapati, A. Kumar and S. L. Jain, ACS Sustainable Chem. Eng., 2018, 6, 7799–7809.

9 C.-L. Tan, M.-Y. Qi, Z.-R. Tang and Y.-J. Xu, ACS Catal., 2023, 13, 8317–8329.

10 L. A. Siddig, R. H. Alzard, A. S. Abdelhamid, T. Ramachandran, H. L. Nguyen, A. P. Paz and A. Alzamly, Inorg. Chem., 2023, 62, 15550–15564.

11 Q. Shi, M.-H. Chen, J. Xiong, T. Li, Y.-Q. Feng and B. Zhang, Chem. Eng. J., 2024, 481, 148301.

12 C. Sarkar, R. Paul, D. Q. Dao, S. Xu, R. Chatterjee, S. C. Shit, A. Bhaumik and J. Mondal, ACS Appl. Mater. Interfaces, 2022, 14, 37621–37636.

13 Y. He, M. Xu, J. Xia, C. Zhang, X. Song, X. Zhao, M. Fu, S. Li and X. Liu, Mol. Catal., 2023, 542, 113134.

14 Z.-R. Jiang, H. Wang, Y. Hu, J. Lu and H.-L. Jiang, ChemSusChem, 2015, 8, 878–885.

15 G. Zhai, Y. Liu, Y. Mao, H. Zhang, L. Lin, Y. Li, Z. Wang, H. Cheng, P. Wang, Z. Zheng, Y. Dai and B. Huang, Appl. Catal., B, 2022, 301, 120793.

16 L. Gong, J. Sun, Y. Liu and G. Yang, J. Mater. Chem. A, 2021, 9, 21689–21694.

17 Q. Yang, C.-C. Yang, C.-H. Lin and H.-L. Jiang, Angew. Chem. Int. Ed., 2019, 58, 3511–3515.